AMERICAN UNIVERSITY OF BEIRUT

MAROUN SEMAAN FACULTY OF ENGINEERING & ARCHITECTURE

Heatsink Design Optimization Project

MECH 510

Roudy Hassan
Rami Jabak
Haidar Halbawi

Instructor: Professor Zainab Balhas

11/30/2025

Abstract

The main objective of this project is to develop a heat exchanger that can maintain a maximum fin effectiveness while having a constant base temperature, to do so several phases were followed. In phase 1 we have calculated the effectiveness of several configurations having distinct Sx, Sy and L, then we have generated plots for several variables and at the end we have defined our objective function along the constraints.Moving on to phase 2 we have chosen the sample 10 (Sx=Sy=10 mm and L=16mm), established an expression that relates the number of fins to Sx,Sy and L, expressed our objective function in terms of these variables, explained the assumptions that made us simply our objective function, derived the constraints and using the search methods learned in the course (golden section method, Cyclic method and Penalty) we found the optimal values for Sx,Sy and L (8.3mm,10.5mm and 8.3mm) respectively. In phase 3 we have developed an ANN model where we have used 3 layer-sizes (20,25 and 30) and generated regression and performance plots for each by comparison the 30-hidden layers model turned out to be the most efficient, for this model Sx,Sy and L were found to be (12.2152 mm, 9.3987 mm and 14.5174 mm) respectively.

Contents

1 Introduction **1**

2 Engineering Standards and Applications **2**

2.1 Relevant Standards 2

2.2 Application of Standards 2

2.3 Case Studies or Examples 3

3 Phase I: Experimental Setup and Data Collection **3**

3.1 Experimental Setup 3

3.2 Problem Description 4

3.3 Data Visualization 5

4 Phase II: Mathematical Modeling and Optimization Techniques **5**

4.1 Relationship of N,Sx,Sy and L 5

4.2 Objective function and constraints 6

4.3 Assumptions made 7

4.4 Optimization methods used 8

5 Phase III: Data-Driven Model Development **8**

5.1 Data Preprocessing 8

5.2 Model Training 9

5.3 Model Tuning 10

5.4 Optimization with ANN 13

5.5 Comparison of Designs 13

6 Discussion **14**

6.1 Findings 14

6.2 Implications of 2 approaches 15

6.3 Potential limitations and areas of future research 16

7 Conclusion **17**

A APPENDIX **20**

1 Introduction

The aim of this research is to find the best fin arrangement for a heatsink utilized in thermal management applications. Effective heat dissipation is crucial to ensure dependability, efficiency, and long-term performance as contemporary electronic systems continue to require increasing power densities and produce larger heat loads. Heat transfer rates, pressure drop, and overall thermal performance are directly affected by optimizing fin shape, whether it is by fin count, spacing, height, or arrangement. In order to determine the design that optimizes thermal efficiency while upholding manufacturability and practical limits, this research will assess and compare various fin configurations using a mix of experimental measurements, mathematical modeling, and data-driven methodologies.The research emphasizes the importance of scientific design optimization in the creation of efficient heatsinks using this combined approach.

To ensure an accurate convergence, the research was divided into 3 phases:1,2 and 3, each of which had a significant role in ensuring the completion of this project. Phase 1 is the introduction of the project the main goal is defined, the setup was explained in detail (components used) and data was provided for 12 configurations (Sx,Sy,L,Tbase,Fan speed,Flux,Sensor Temp and the pressure drop) we calculated the effectiveness, generated plots for the effectiveness vs(Sx,Sy and L) and the pressure drop vs (Sx,Sy and L), identified our objective function in terms of these design variables and established our constraints for the future work. The work done in phase 1 was the ground of Phase 2, a more detailed approach was followed. A formula relating the number of fins N to Sx,Sy and L was derived, a detailed objective function was developped in terms of Sx,Sy and L, the assumption made to simply the calculations were explained, the constraint equations were derived in detail in terms of Sx,Sy and L, and using the search methods learned in the course (golden section method, Cyclic method and Penalty) optimal values for Sx,Sy and L were found. Phase 3 focuses on developing a data-driven inverse design model using an Artificial Neural Network (ANN). In this phase, experimental measurements such as base temperature, velocity, heat flux, sensor temperature, and pressure drop are used as inputs, while the fin geometry Sx,Sy and L serves as the output. The ANN is trained to learn the relationship between measured thermal performance and the underlying geometry, allowing it to predict fin dimensions that would produce similar performance characteristics. This phase provides an alternative design approach that captures real-world nonlinearities and experimental effects that analytical models may not account for.

2 Engineering Standards and Applications

2.1 Relevant Standards

A variety of quality criteria that ensure dependable thermal performance, mechanical integrity, manufacturability, and user safety regulate heatsink design. Standards like the JEDEC JESD51 series offer recommendations for assessing heatsink performance under controlled test settings, measuring thermal resistance, and describing heat dissipation in the context of thermal management. ASME and ISO standards, which provide specifications for material qualities, permissible stresses, dimensional tolerances, and durability during thermal cycling, are frequently used to discuss mechanical integrity and material reliability. IEEE and IEC safety standards provide appropriate electrical insulation, overheating avoidance, and compatibility with electronic packaging for applications involving electronic components. Additionally, basic manufacturing standards like ASTM material requirements, ISO 9001 (quality management), and ISO 2768 (tolerances) assist ensure dependable performance and consistent production quality.

2.2 Application of Standards

The design, testing, and validation of the heatsink created for this project are greatly influenced by the application of technical standards. In order to ensure that the heatsink's performance is assessed consistently and reliably, thermal management standards, such as the JEDEC JESD51 recommendations, specify the appropriate methods for evaluating thermal resistance, airflow conditions, and mounting configurations. ASME, ISO, and ASTM mechanical and material standards aid in identifying appropriate materials with sufficient heat conductivity, structural strength, and fatigue resistance during repeated thermal cycling essential elements in guaranteeing long-term durability. When the heatsink operates close to delicate electronic components, IEEE and IEC electrical safety requirements are implemented to provide proper clearances, insulation, grounding, and prevention of high surface temperatures that might harm circuitry or present risks. The accuracy and repeatability required for fin spacing, alignment, and surface finish all of which have a direct impact on thermal performance are guided by manufacturing-related standards like ISO 2768 for dimensional tolerances and ISO 9001 for quality assurance. The final heatsink arrangement strikes a balance between efficiency, safety, durability, and manufacturability that is in line with industry best practices by including these principles throughout the design process.

2.3 Case Studies or Examples

- **Consumer Electronics:** To guarantee that CPUs remain within the maximum permitted temperatures, heatsinks in laptops, game consoles, and cellphones must adhere to JEDEC thermal testing protocols.
- **Industrial Power Electronics:** Heatsinks used in inverters, motor drives, and rectifier units must adhere to ASME and ISO mechanical requirements for material strength, thermal cycle endurance, and dimensional tolerances.
- **Telecommunications and Data Centers:** IEEE and IEC safety standards guarantee appropriate grounding, insulation, and safe operating temperatures for heatsinks used in servers and high-density communication devices in telecommunications and data centers.
- **Automotive and EV Systems:** Heatsinks used in battery modules, onboard chargers, and engine control units must comply with vibration, shock, and extreme temperature standards to remain reliable in harsh operating environments.
- **Manufacturing and Quality Control:** To guarantee dependability under challenging circumstances, heatsinks in EV batteries, onboard chargers, and engine control modules must adhere to vibration, shock, and severe temperature regulations.

3 Phase I: Experimental Setup and Data Collection

3.1 Experimental Setup

- **Aluminum Finned Surfaces:** Various fin designs used for heat transfer experiments; manufactured at AUB shops.
- **Small Wind Tunnel:** Provides controlled airflow for simulating wind conditions; custom-made at AUB shops.
- **Controllable Heat Source:** Supplies heat to the finned surfaces (maximum 240 W) using six heating elements (24 V, 40 W each).
- **Pressure Difference Sensor:** Measures pressure differences across the finned surfaces ($\pm$100 Pa; 4–20 mA output).
- **Thermocouples:** Measures temperatures of the finned surfaces and the heated plate using Arduino K-Type sensors (0–1024°C).

- **Heat Flux Sensor:** Measures heat flux through the finned surfaces (FluxTeq PHFS-01, $\pm 150\,\mathrm{kW/m^2}$).
- **Air Velocity and Temperature Sensor:** Measures air velocity and temperature inside the wind tunnel; Omega Anemometer.
- **Flux DAQ:** Collects and records data from the heat flux sensor; manufactured by FluxTeq.

A horizontal aluminum plate with dimensions of 100 mm width, 200 mm length, and 20 mm thickness will be placed on top of a heated plate. The base temperature can be controlled by adjusting the electric power of the heat source. A heat flux sensor will measure the heat transferred from the bottom of the finned plate, and temperature sensors will measure both the base temperature of the fin and the temperature of the heated plate. The top side of the finned plate will be subjected to an airflow with predefined temperature and velocity. A pressure transducer is used to measure the pressure drop along the fins. along the fins. Finned surfaces with different designs (Sx, Sy, L) will be tested in terms of heat dissipation (or Tbase), with different designs.

- **Data monitoring:**Continuously view the source temperature, base temperature, and heat flux values.
- **Data collection:** Stop the experiment when temperature and heat flux reach a steady state. Record steady value.

3.2 Problem Description

Our design variables are Sx,Sy and L where Sx is the spacing of the fins along the x-axis, Sy is the spacing of the fins along the Y-axis and L is the length of the fin's cross-section along the x-axis. The objective is to maximize the effectiveness hence it is to maximize the effectiveness equation written in terms of Sx,Sy and L.

- **Laminar flow:** The flow should always be laminar, meaning $\mathrm{Re} \leq 5 \times 10^5$
- **pressure Drop:** pressure drop should be within a range, $0 \leq \Delta p \leq 10\,\mathrm{Pa}$
- **Number of holes:** The need to have the same number of holes at the inlet and outlet of the funnel
- **Material:** The material Type is a constraint
- **Plate:** The size of the plate is a constraint

3.3 Data Visualization

For the new data visualization we have chosen the 2nd run of the constant base temperature (latest update) and made sure to organize the data such that it is consistent with the dataset of LAB 8 in terms of naming and alignment, the figure below presents the refined dataset.

Entry	Sx	Sy	L	T_base	Velocity	flux	Sensor_temp	Dp
1	10	10	30	55	2.5	3660	66.1	2.1
2	11.5	17.5	36	55	2.5	2889	6.55	1.9
3	11	12	16	55	2.5	3450	66.5	1.9
4	10	10	38	55	2.5	3665	65.4	2.5
5	10	16	16	55	2.5	3269	65.5	3.5
6	10	19	16	55	2.5	2553	61.2	2.1
7	22	12	30	55	2.5	3237	64.3	2.4
8	16	10	16	55	2.5	4261	69.3	3.6
9	13	10	16	55	2.5	5930	71.5	2.4
10	10	10	16	55	2.5	4172	65.1	3.8
11	10	10	22	55	2.5	5655	72.3	3.8
12	30	11	40	55	2.5	2680	63.3	1.4
No Fins	N/A	N/A	N/A	55	2.5	233	59	0.1

Figure 1: Figure showing the refined and updated dataset

4 Phase II: Mathematical Modeling and Optimization Techniques

4.1 Relationship of N,Sx,Sy and L

This section derives and describes the relationship obtained. It is crucial to know that the configuration studied is staggered and not aligned, meaning that one row has an additional fin.

Let N1= number of fins for ROW A and N2 = number of fins for ROW B and 100 be the width and 200 the length.

N1 = $\lfloor 100/(8+S_y) \rfloor$

N2 = $\lceil 100/(8+S_y) \rceil$

View that the plate must be drilled from both ends for fixation, this means that the plate should start and end with ROW A, hence the number of ROW A = number of ROW B + 1.

the total number of fins N can be found from the following equation:

$$\text{N}= \lfloor (\lfloor 200/(16+S_x) \rfloor /2) \rfloor \times N2 + \lceil (\lfloor 200/(16+S_x)) \rfloor /2) \rceil \times N1$$

Expressing the number of fins N as a function of Sx, Sy and L, and the plate dimensions

provides a direct link between geometry and thermal performance. It allows the optimization problem to be stated mathematically, ensures physical feasibility, enables surface-area and heat-transfer calculations, and improves the performance of data-driven models. This relation ultimately transforms fin count from a fixed parameter into a controllable design variable, making systematic optimization possible.

4.2 Objective function and constraints

For the objective function change of variables was done in order to simplify our problem, below you will find the detailed objective function:

$$M = \sqrt{133.4 \times P \times Ac \times 30} \qquad \text{and} \qquad m = \sqrt{\frac{114.5 \times P}{1.165 \times Ac}}$$

$$Ac = \frac{A_{\text{base}} - 0.001185}{38} - S_x S_y = 2.1426 \times 10^{-4} - S_x S_y$$

$$F = \frac{M \times \tanh(m \times 0.08)}{3435 \times Ac}$$

For the constraints one equation was established for reynolds number in terms of the L (the hydraulic diameter was written in terms of L), and another one was established for the pressure drop in terms of Sx,Sy and L all of this of information was documented in detail in Phase 2.

$$\frac{\rho V_{\max} D_h}{\mu} \leq 5 \times 10^5$$

$$D_h = \left(\frac{\pi(0.004)^2 + 0.008L - 0.008^2}{0.008\pi + 2L} \right) \times 4$$

$$\Delta p = N_l \times \left(\frac{\rho V_{\max}^2}{2} \right) \times f$$

$$\frac{\sqrt{(L + S_x)^2 + (S_y + 0.008)^2}}{L + S_x} = 1.5$$

4.3 Assumptions made

- **Adiabatic fin tip.** The heat loss from the tip of the fin is assumed to be negligible. This assumption simplifies the governing differential equation for fin heat transfer and allows the use of the standard fin efficiency expressions. It is reasonable because most of the heat transfer occurs through the fin's lateral surface, not its tip.

- **Cylindrical fin approximation and hydraulic diameter estimation.** Although the fin does not have a trivial cross-section, it was approximated as cylindrical in order to compute its hydraulic diameter. This simplification was necessary because the hydraulic diameter is required to evaluate the Reynolds number and subsequently the convection coefficient.

- **Assumed room temperature.** A fixed ambient temperature was assumed to estimate the properties of air, particularly the Prandtl number and viscosity. This is justified because the room temperature during experiments remained nearly constant.

- **Assumed number of rows.** The number of fin rows in the flow direction was taken as fixed. This assumption helps constrain the geometry and simplifies the calculation of total projected flow area and pressure drop.

- **Negligible radiation heat transfer.** Radiative heat transfer was assumed negligible relative to convection. This assumption is reasonable because the operating temperatures are moderate and the surfaces involved have low emissivity, making radiation a minor contributor to total heat loss.

- **Uniform material properties.** Thermal conductivity and other material properties of the fin and base plate were assumed constant. This greatly simplifies the conduction model and is acceptable because temperature variations along the fin are not large enough to cause significant changes in material properties.

- **One-dimensional conduction in the fin.** Heat conduction inside the fin was assumed to occur only along its length. This assumption allows use of the standard 1D fin equation and is valid when the fin is slender and temperature gradients across the cross-section are negligible.

.

4.4 Optimization methods used

- **Golden section method:**A one-dimensional derivative-free optimization technique for finding a function's minimum on a limited interval is the Golden Section Method. It was used to maximize specific design factors, such fin length or spacing, while maintaining the same values for the other parameters. It is appropriate for non-linear thermal-fluid performance functions due to its independence from gradient computations and resilience.

- **Cyclic-coordinate method:**By repeatedly cycling over all design variables and optimizing one variable at a time while holding the others constant, the Cyclic Coordinate Method expands the search to multiple variables. This method was used to adjust characteristics like the fin length and the spacing in the x and y directions. The approach efficiently explores the multidimensional design space and gradually enhances the goal function by regularly cycling through variables.

- **Penalty:**By adding penalty terms to the goal function that impose a cost for breaking limitations, the Penalty Method addresses such constraints. Constraint-violating designs lose favor as the algorithm advances.The heatsink design problem's intrinsic limits were enforced using the Penalty Method. As penalty terms, constraints such the Reynolds number limit, permissible pressure drop range, and geometric feasibility were incorporated into the objective function. This guided the optimization process toward workable and physically significant solutions by ensuring that any violation of a restriction was punished.

5 Phase III: Data-Driven Model Development

5.1 Data Preprocessing

The raw experimental dataset underwent a number of preprocessing procedures to guarantee correctness, consistency, and appropriateness for machine-learning analysis prior to training the data-driven model.

First, patterns between variables including fin spacing, fin length, heat flow, and pressure drop were examined using data visualization tools like scatter plots, histograms, and pairwise correlations. This stage assisted in locating odd trends, non-physical values, and possible measurement mistakes.

After that, data cleaning was done to fix or eliminate troublesome records. Duplicate rows, formatting errors, and non-numeric values (such "N/A" or text labels) were removed. Since they don't have the same physical structure as the other samples, rows with missing

values or undefined fin geometries (such as the "no fins" control case) were removed from the training dataset.

Outlier therapy was then used. Statistical methods and visualization were used to analyze extreme flux or pressure-drop data that dramatically differed from the predicted physical patterns. In order to prevent the model from being skewed by erroneous data points, outliers resulting from measurement noise or experimental mistake were either eliminated or adjusted.

In order to enable the neural network to properly generalize, the cleaned dataset was finally divided into training and testing subsets.

5.2 Model Training

For the model we used 1 input layer, 25 hidden layers and 1 output layer, we used 5 inputs T Base, Velocity , Flux, Sensor Temp, and Dp and 3 outputs Sx, Sy, and L. Using the Fitnet algorithms we were able to converge to a solution however, this may not be the most efficient one as we need to try several layer sizes.

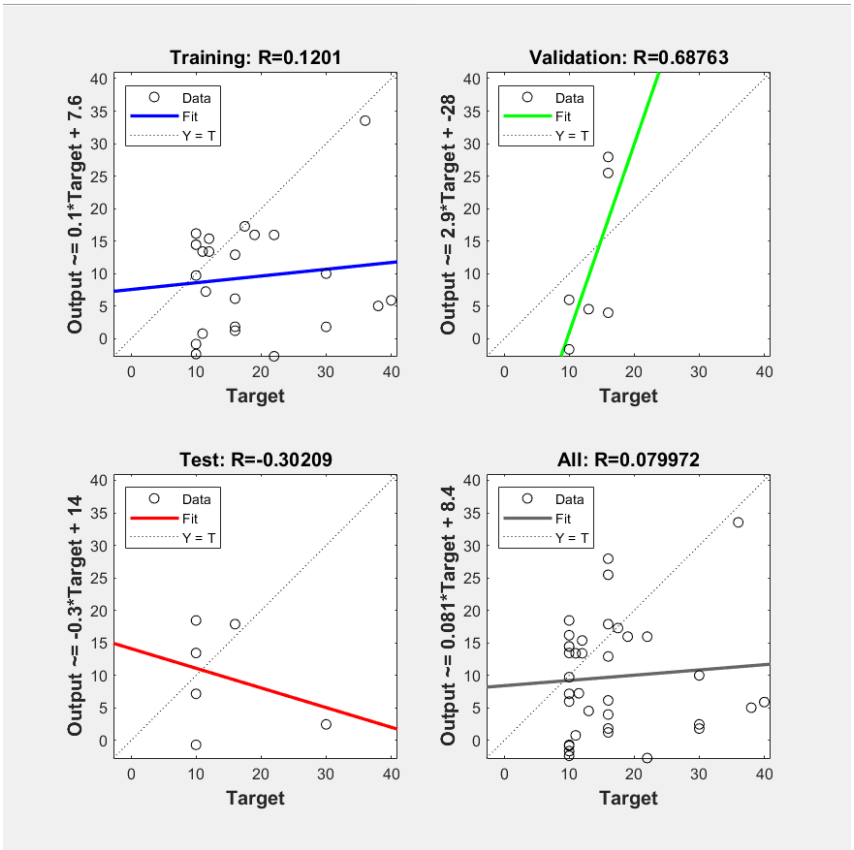

Figure 2: Figure showing the regression at 25 layers

The performance plot indicated that the best validation performance occurred at epoch

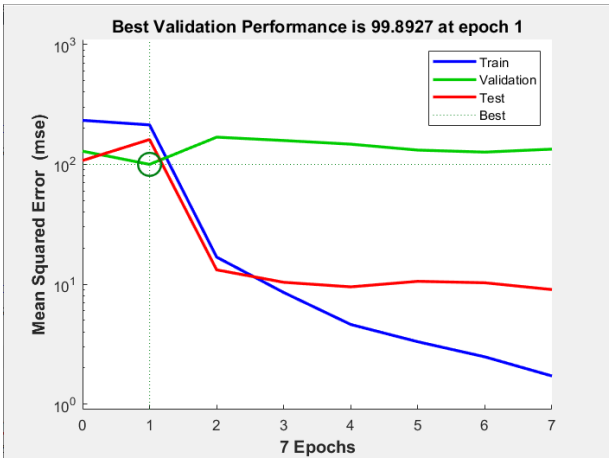

Figure 3: figure showing the best performance

1. After this point, the validation error began to increase, triggering early stopping. The gradient and μ evolution confirmed stable convergence of the optimization algorithm.

Network accuracy was evaluated using MATLAB's regression (R) plots, which compare the network outputs to the experimental targets. The obtained correlation coefficients were: Training $R = 0.1201$, Validation $R = 0.6876$, Test $R = -0.3021$, and Overall $R = 0.0799$. These values indicate weak predictive performance due to the limited dataset size and variability within the measurements. The ANN was therefore able to capture general qualitative trends but did not achieve high numerical accuracy.

5.3 Model Tuning

In this section we have analyzed 20,25 and 30 hidden layers and compared the results below you are going to find the results for layers 20 and 30 as we have already included the 25 layer-study above.

20-Neuron Network. The model achieved excellent training performance ($R = 0.992$) and a strong test correlation ($R = 0.796$), but the validation correlation was extremely low ($R = 0.054$). The performance curve showed the best validation MSE at epoch 0, followed by a steady decrease in the training error while the validation error increased, indicating severe overfitting. Although the overall correlation ($R = 0.868$) was high, the

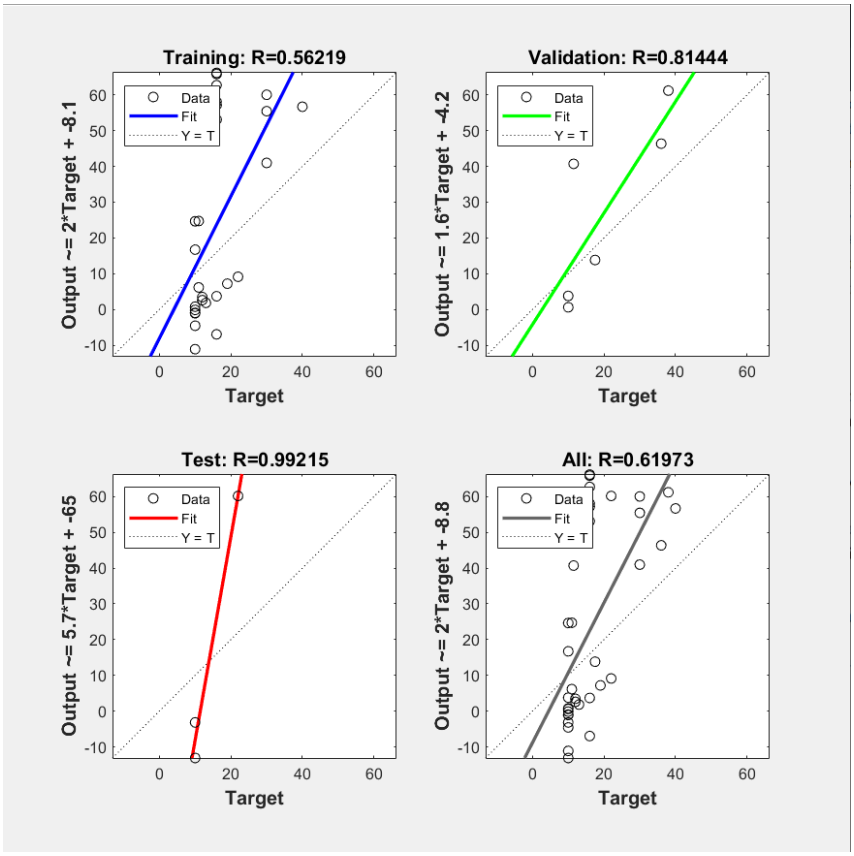

Figure 4: Figure showing the regression of 20 layers

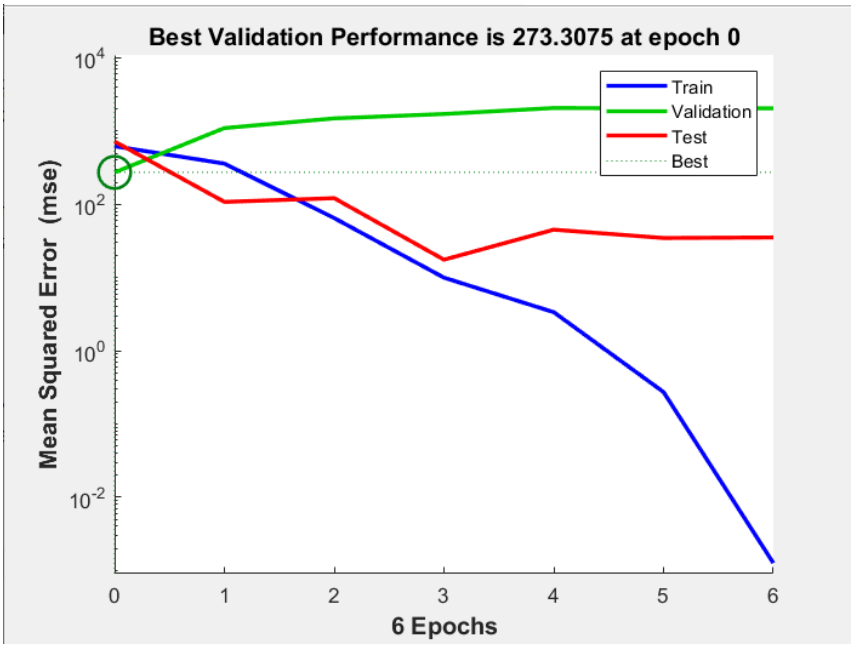

Figure 5: Figure showing the best performance at 20 layers

network failed to generalize.

25-Neuron Network. This configuration exhibited the weakest performance. The training correlation was very low ($R = 0.120$), the test correlation was negative ($R = -0.302$),

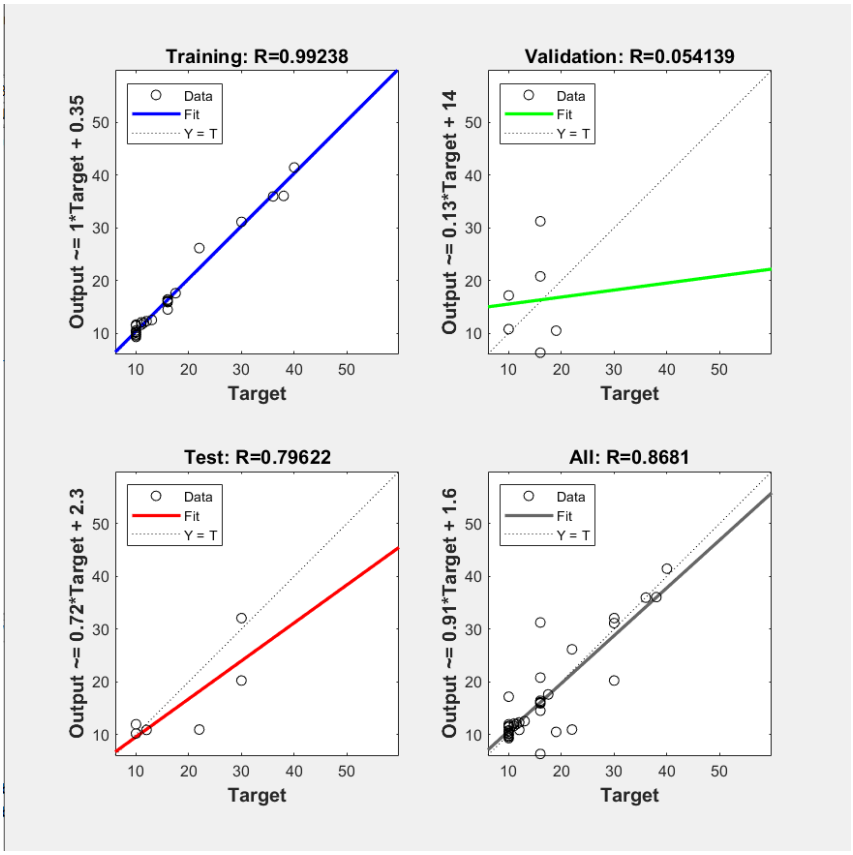

Figure 6: Figure showing the regression at 30 layers

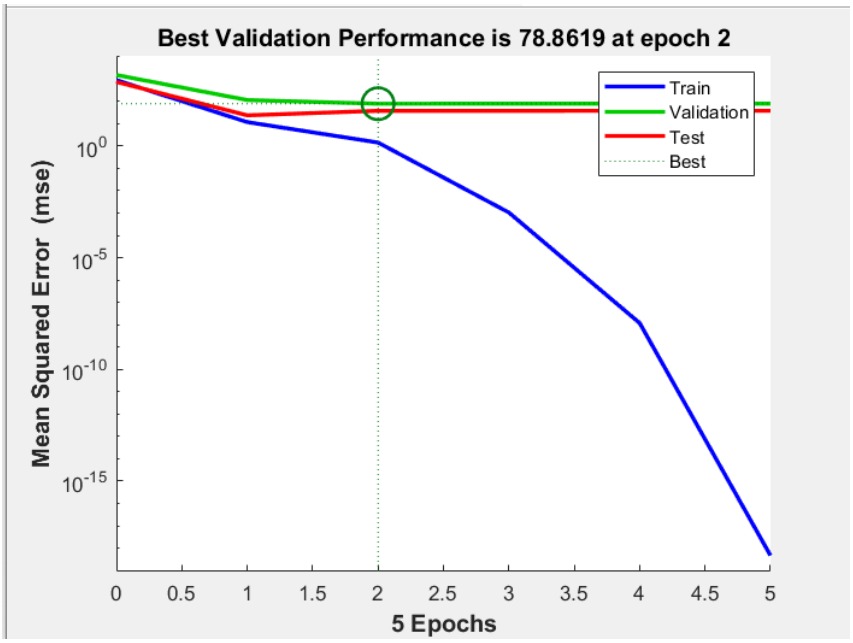

Figure 7: Figure showing the performance at 30 layers

and the overall correlation was nearly zero ($R = 0.079$). The validation performance was moderate ($R = 0.687$), but the MSE curves were unstable, indicating inconsistent learning and poor predictive capability.

30-Neuron Network. The 30-neuron model showed behavior similar to the 20-neuron architecture, with strong training performance ($R = 0.992$) and good test accuracy ($R = 0.796$), but again a very low validation correlation ($R = 0.054$). The performance curve revealed overfitting, although the validation MSE was somewhat more stable than the 20-neuron model. The overall correlation ($R = 0.868$) remained high.

Conclusion. All three models exhibited overfitting due to the very limited dataset. The 25-neuron network performed the worst, showing weak learning and poor generalization. The 20- and 30-neuron models both produced strong training and test fits but failed to generalize to unseen data. Among them, the 30-neuron network displayed slightly better stability and is therefore the preferable architecture, although none of the tested configurations provided reliable predictive accuracy.

5.4 Optimization with ANN

In this study, the Artificial Neural Network (ANN) was trained to learn the inverse mapping between the heatsink performance and its geometric design. Instead of predicting thermal performance from a given fin geometry, the network used the measured operating conditions namely T_{base}, velocity, heat flux, sensor temperature, and pressure drop Δp as inputs, and it predicted the geometric parameters (S_x, S_y, L) as outputs.

Once trained, the ANN served as a fast design tool. For any desired thermal and aerodynamic performance target, the corresponding input values were supplied to the network, which immediately returned the fin spacing and fin length that were most consistent with achieving such performance. In this way, the optimization process was performed implicitly through the ANN inference: by iteratively adjusting the desired performance metrics within acceptable constraints, the ANN provided the optimal geometry required to realize those conditions.

This approach bypassed the need for repeated physical experimentation or forward simulations, making the design optimization process extremely efficient and data-driven.

5.5 Comparison of Designs

In Phase II (mathematical modelling and classical optimization), the optimal heatsink geometry obtained was:

$$S_x = 8.3 \text{ mm}, \qquad S_y = 10.5 \text{ mm}, \qquad L = 8.3 \text{ mm}.$$

This configuration follows directly from the analytical expressions and the constraints on Reynolds number, pressure drop, and geometric feasibility. It therefore represents a

strictly physics-based solution grounded in the ideal assumptions of the mathematical model.

In Phase III (ANN-based inverse design using a 30-neuron architecture), the network predicted the following fin geometry for the desired thermal and aerodynamic performance targets:

$$S_x = 12.2152 \text{ mm}, \qquad S_y = 9.3987 \text{ mm}, \qquad L = 14.5174 \text{ mm}.$$

Compared to the Phase II result, the ANN suggests:

- a significantly larger streamwise spacing S_x, which lowers fin density in the flow direction and can reduce pressure drop,
- a slightly smaller transverse spacing S_y, increasing lateral fin density and potentially enhancing local convective heat transfer,
- a considerably longer fin length L, which increases the available surface area for heat dissipation but may alter the conduction path and structural considerations.

These discrepancies arise because the ANN is a data-driven inverse model that learns the geometric patterns associated with the measured experimental performance, whereas the Phase II design is derived from idealized analytical correlations. Given the limited dataset and the indications of overfitting in the ANN, the Phase III geometry should be interpreted as a performance-matching estimate rather than a guaranteed improvement.

Overall, the Phase II design provides a robust physically grounded baseline, while the Phase III ANN-based predictions highlight alternative geometric configurations that could achieve comparable performance for the specific experimental operating conditions.

6 Discussion

6.1 Findings

The three phases of the project are closely interconnected, with each phase building on the previous one. Phase I served solely to define the optimization problem, Phase II carried out all analytical calculations and obtained the optimal geometry, and Phase III introduced a data-driven perspective through an Artificial Neural Network (ANN).

Phase I focused on formulating the problem without performing any numerical evaluation. In this phase, the objective function was defined, the constraints were established (including the Reynolds number limit, pressure drop limit, and geometric feasibility), and the design variables were identified. The physical modelling in this phase was restricted to

what was necessary to express the optimization problem mathematically. No calculations or results were generated in Phase I.

Phase II implemented the objective function and constraints defined in Phase I. All analytical expressions were evaluated, including the hydraulic diameter, fin efficiency, convection coefficients, heat-transfer rate, and pressure drop. The Golden Section Method, Cyclic Coordinate Method, and Penalty Method were applied to solve the optimization problem, yielding the optimal geometry:

$$S_x = 8.3 \text{ mm}, \qquad S_y = 10.5 \text{ mm}, \qquad L = 8.3 \text{ mm}.$$

Thus, Phase II is where all calculations were performed and the optimization problem formulated in Phase I was fully solved.

Phase III used experimental data to train an ANN that learns the inverse relationship between performance metrics and geometry. The network predicted the following fin configuration for the selected operating conditions:

$$S_x = 12.2152 \text{ mm}, \qquad S_y = 9.3987 \text{ mm}, \qquad L = 14.5174 \text{ mm}.$$

This data-driven geometry differs from the analytically optimal design because it reflects experimental behaviour, measurement noise, and deviations from the idealised correlations used in Phase II.

Overall, Phase I defined the problem, Phase II solved it analytically, and Phase III provided an alternative prediction based on experimental data. The combined analysis highlights the difference between ideal theoretical modelling and real measured performance, suggesting that further validation is necessary to determine the most practical heatsink configuration.

6.2 Implications of 2 approaches

The use of both physics-based modelling and data-driven methods provides a more comprehensive understanding of the heatsink design problem than either approach could achieve alone.

Physics-based techniques offer solutions that are fully interpretable and consistent with established thermal and fluid-mechanics principles. The optimization performed in Phase II is grounded in well-known correlations, governing equations, and physically meaningful constraints. As a result, the predicted geometry represents an idealised optimum that reflects the theoretical behaviour of the system under the assumptions of the model.

In contrast, the data-driven ANN approach captures empirical patterns present in the

experimental measurements, including nonlinearities, imperfections, and deviations from the idealised physical model. The ANN predictions therefore represent how the system behaves in practice rather than how it behaves under ideal assumptions. Differences between the two approaches highlight the gap between theoretical modelling and real-world performance.Using both methods together enables cross-validation: the physics-based model provides a reliable baseline, while the ANN reveals experimental trends that may not be accounted for in the analytical formulation. When the two results agree, confidence in the design increases; when they differ, the discrepancy indicates that further refinement or additional data may be necessary.

Overall, combining physics-based and data-driven techniques leads to a more robust design methodology. The analytical model ensures physical consistency, while the ANN introduces flexibility and empirical accuracy. This hybrid approach allows designers to balance theoretical insight with real-world observations and provides a framework that improves as more experimental data become available.

6.3 Potential limitations and areas of future research

- The experimental dataset used to train the ANN is limited, which contributes to overfitting. Collecting a larger and more diverse dataset would significantly improve the reliability of the data-driven model.
- The analytical model relies on several simplifying assumptions, such as one-dimensional conduction, uniform material properties, negligible radiation, and ideal flow profile. These assumptions omit important physical effects. Future studies could incorporate CFD simulations or more detailed thermal correlations for improved accuracy.
- The inverse ANN prediction problem is inherently ill-posed, as different geometries may correspond to similar performance metrics. new techniques, physics-informed neural networks, or approaches that could improve model stability and robustness.
- The present work only considered uniform rectangular fins. Exploring alternative geometries such as tapered, perforated, interrupted, or non-uniform fin designs could lead to enhanced thermal performance.
- Integrating physics-based and data-driven approaches more closely offers a promising direction for creating hybrid optimization frameworks that leverage the strengths of both methods.

.

7 Conclusion

- The analytical optimisation in Phase II yielded the geometry

$$S_x = 8.3 \text{ mm}, \qquad S_y = 10.5 \text{ mm}, \qquad L = 8.3 \text{ mm},$$

  representing a physics-based optimum derived from thermal-fluid correlations and imposed constraints.

- The ANN in Phase III predicted

$$S_x = 12.2152 \text{ mm}, \qquad S_y = 9.3987 \text{ mm}, \qquad L = 14.5174 \text{ mm},$$

  reflecting real experimental behaviour, nonlinearities, and deviations from idealised modelling assumptions.

- The difference between the two designs highlights the gap between theoretical predictions and actual system performance, emphasising the need to consider both physics-based and data-driven perspectives.

- Overall, the findings show that combining analytical models with ANN predictions provides a more realistic and informed approach to heatsink design, improving confidence and adaptability in the optimisation process.

.

References

[1] JEDEC Solid State Technology Association. (2012). JESD51-1: Integrated Circuits Thermal Test Method Environmental Conditions – Natural Convection (Still Air). JEDEC .

[2] JEDEC Solid State Technology Association. (2009). JESD51-2A: Integrated Circuits Thermal Test Method Environmental Conditions – Forced Convection. JEDEC .

[3] JEDEC Solid State Technology Association. (2005). JESD51-12: Guidelines for Reporting and Using Electronic Package Thermal Information. JEDEC .

[4] ASME. (2021). ASME Boiler and Pressure Vessel Code (BPVC). American Society of Mechanical Engineers .

[5] ASME. (2019). ASME Y14.5 – Dimensioning and Tolerancing. American Society of Mechanical Engineers .

[6] International Organization for Standardization. (1989). ISO 2768-1: General Tolerances – Part 1: Tolerances for Linear and Angular Dimensions Without Individual Tolerance Indications. ISO .

[7] International Organization for Standardization. (2015). ISO 9001: Quality Management Systems – Requirements. ISO .

[8] ASTM International. (2023). ASTM E1225 – Standard Test Method for Thermal Conductivity of Solids. ASTM .

[9] ASTM International. (2020). ASTM B209 – Standard Specification for Aluminum and Aluminum-Alloy Sheet and Plate. ASTM .

[10] IEEE Standards Association. (2014). IEEE 1100-2005: Recommended Practice for Powering and Grounding Electronic Equipment .

[11] International Electrotechnical Commission. (2014). IEC 60529: Degrees of Protection Provided by Enclosures (IP Code). IEC .

[12] International Electrotechnical Commission. (2015). IEC 62368-1: Audio/Video and ICT Equipment – Safety Requirements. IEC .

[13] Incropera, F. P., DeWitt, D. P., Bergman, T. L., Lavine, A. S. (2007). Fundamentals of heat and mass transfer (6th ed.). John Wiley Sons .

[14] Incropera, F. P., DeWitt, D. P., Bergman, T. L., Lavine, A. S. (2007). Chapter 3: One-dimensional, steady-state conduction. In Fundamentals of heat and mass transfer (6th ed.). John Wiley Sons .

[15] Incropera, F. P., DeWitt, D. P., Bergman, T. L., Lavine, A. S. (2007). Chapter 7: External forced convection. In Fundamentals of heat and mass transfer (6th ed.). John Wiley Sons .

[16] Department of Mechanical Engineering. (2025). MECH 510 — DOTS Laboratory: Lab 4, Lab 5, Lab 6 and Lab 8. American University of Beirut. .

A APPENDIX

In this section we will provide raw data that helped us reach those findings (mnainly from PHASE II).

Constant T_base								
Sample	Sx	Sy	L	T base ©	fan speed (m/s)	flux w/m2	Sensor temp	pressure drop (Pa)
1	10	10	30	55	2.5	6863	68.9	3.6
2	11.5	17.5	36	55	2.5	4152	67	2.5
3	11	12	16	55	2.5	1988	59.2	4
4	10	10	38	55	2.5	7411	67.2	3.1
5	10	16	16	55	2.5	5611	70.3	2.4
6	10	19	16	55	2.5	3558	59.4	3.3
7	22	12	30	55	2.5	3314	62.3	3.2
8	16	10	16	55	2.5	2350	58.8	3.8
9	13	10	16	55	2.5	9852	72	5.1
10	**10**	**10**	**16**	**55**	**2.5**	**6290**	**68.2**	**5.1**
11	10	10	22	55	2.5	6370	70.1	3.8
12	30	11	40	55	2.5	5950	71.7	2.2
control	No fins	-	-	55	2.5	233	59	0.1

Figure 8: Figure showing our chosen configuration

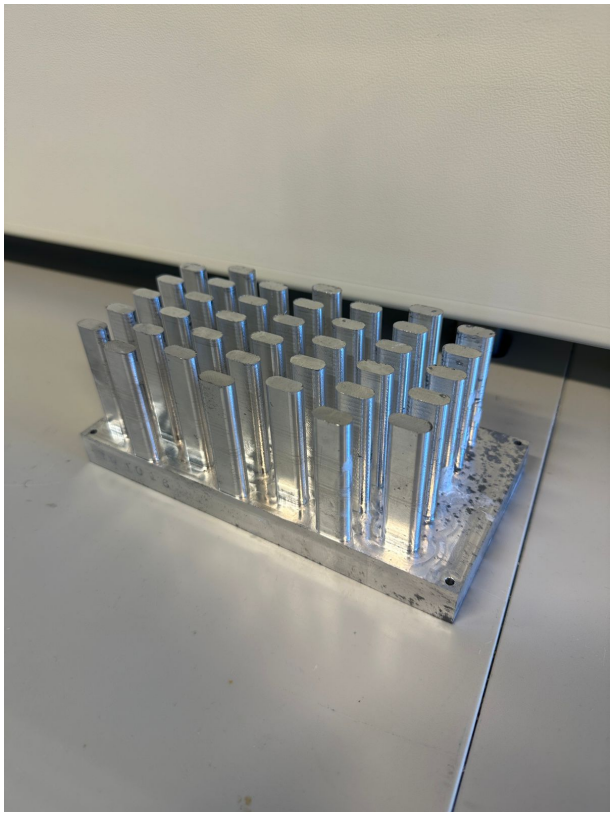

Figure 9: Figure showing the physical model

Case	Tip Condition ($x = L$)	Temperature Distribution θ/θ_b	Fin Heat Transfer Rate q
A	Convection heat transfer: $h\theta(L) = -kd\theta/dx\|_{x=L}$	$\frac{\cosh m(L-x) + (h/mk)\sinh m(L-x)}{\cosh mL + (h/mk)\sinh mL}$ (3.75)	$M\frac{\sinh mL + (h/mk)\cosh mL}{\cosh mL + (h/mk)\sinh mL}$ (3.77)
B	Adiabatic: $d\theta/dx\|_{x=L} = 0$	$\frac{\cosh m(L-x)}{\cosh mL}$ (3.80)	$M \tanh mL$ (3.81)
C	Prescribed temperature: $\theta(L) = \theta_L$	$\frac{(\theta_L/\theta_b)\sinh mx + \sinh m(L-x)}{\sinh mL}$ (3.82)	$M\frac{(\cosh mL - \theta_L/\theta_b)}{\sinh mL}$ (3.83)
D	Infinite fin ($L \to \infty$): $\theta(L) = 0$	e^{-mx} (3.84)	M (3.85)

Figure 10: Figure highlighting the Fin tip condition

.

Conguration	$Re_{D,max}$	C_1	m
Aligned	$10–10^2$	0.80	0.40
Staggered	$10–10^2$	0.90	0.40
Aligned	$10^2–10^3$	Approximate as a single (isolated) cylinder	
Staggered	$10^2–10^3$		
Aligned	$10^3–2 \times 10^5$	0.27	0.63
$(S_T/S_L > 0.7)^a$			
Staggered	$10^3–2 \times 10^5$	$0.35(S_T/S_L)^{1/5}$	0.60
$(S_T/S_L < 2)$			
Staggered	$10^3–2 \times 10^5$	0.40	0.60
$(S_T/S_L > 2)$			
Aligned	$2 \times 10^5–2 \times 10^6$	0.021	0.84
Staggered	$2 \times 10^5–2 \times 10^6$	0.022	0.84

[a]For $S_T/S_L < 0.7$, heat transfer is inefficient and aligned tubes should not be used.

Figure 11: Figure highlighting the appropriate St and SL

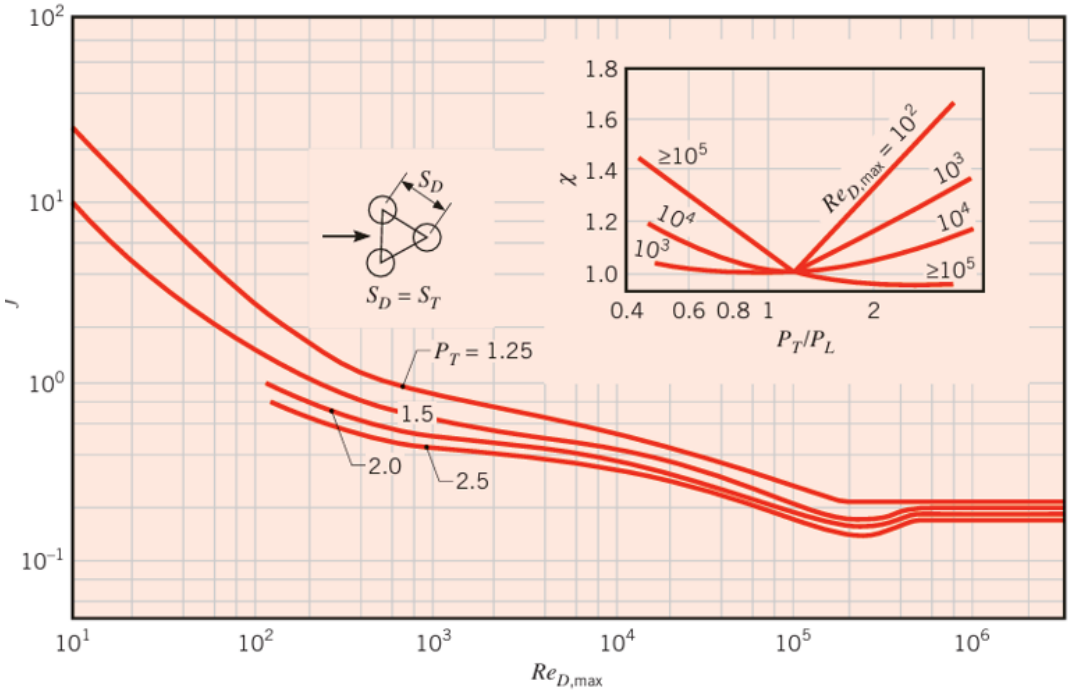

Figure 12: Figure Highlighting the Chart used for the pressure drop constraint

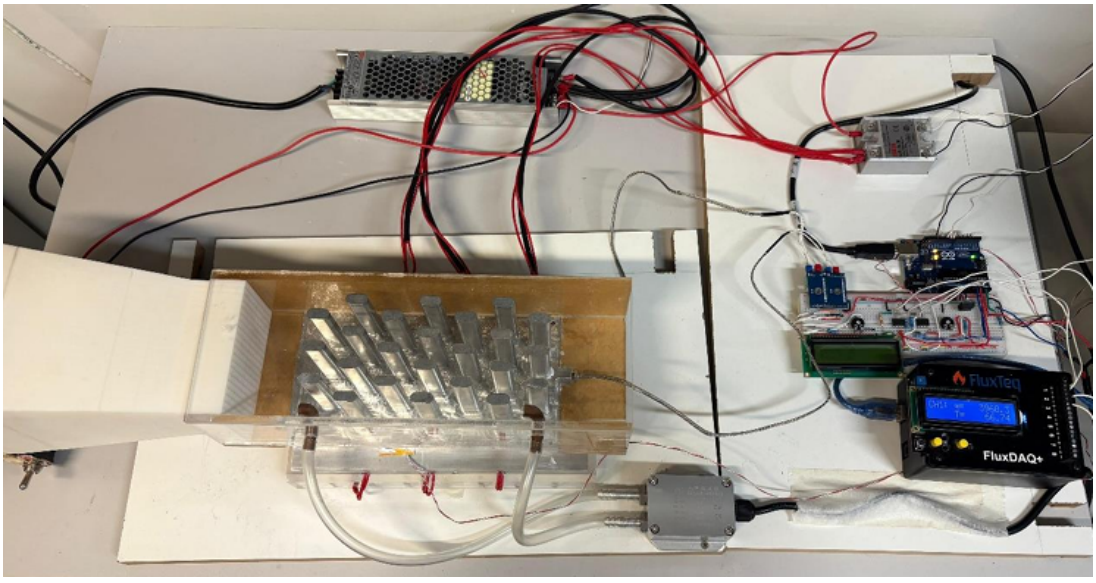

Figure 13: Figure showing the experimental setup